Transition-Metal Complexes with Sulfur Ligands. 88.[1] Dependence of Spin State, Structure, and Reactivity of [Fe^{II}(L)('N_HS_4')] Complexes on the Coligand L (L = CO, N_2H_2, N_2H_4, NH_3, Pyridine, $NHCH_3NH_2$, CH_3OH, THF, $P(OCH_3)_3$, $P(OPh)_3$): Model Complexes for Iron Nitrogenases ('$N_HS_4'^{2-}$ = Dianion of 2,2'-Bis[(2-mercaptophenyl)thio]diethylamine)

Dieter Sellmann,*,† Wolfgang Soglowek,† Falk Knoch,† Gerhard Ritter,‡ and Joachim Dengler‡

Institut für Anorganische Chemie der Universität Erlangen-Nürnberg, Egerlandstrasse 1, W-8520 Erlangen, Federal Republic of Germany, and the Physikalisches Institut der Universität Erlangen-Nürnberg, Erwin-Rommel-Strasse 1, W-8520 Erlangen, Federal Republic of Germany

Received January 29, 1992

In search of complexes exhibiting functional *and* structural characteristics of the active centers of nitrogenases, the Fe^{II} complexes [Fe(L)('N_HS_4')] with the pentadentate amine–thioether–thiolate ligand '$N_HS_4'^{2-}$ (L = N_2H_4, CH_3OH, THF, pyridine, NH_3, $NHCH_3NH_2$, $P(OMe)_3$, $P(OPh)_3$; '$N_HS_4'^{2-}$ = dianion of 2,2'-bis[(2-mercaptophenyl)thio]diethylamine), [Fe('N_HS_4')]$_x$, and the free ligand ['N_HS_4'–H_2]·HCl were synthesized and characterized. The molecular structures of the complexes with L = N_2H_4, NH_3, and CH_3OH have been elucidated by X-ray structure analyses. The crystal data for [Fe(N_2H_4)('N_HS_4')] (**1a**) are orthorhombic space group *Pbca*, a = 1102.1 (7), b = 1567.2 (8), c = 2206.6 (14) pm, Z = 8, and R/R_w = 0.046/0.046. The crystal data for [Fe(CH_3OH)('N_HS_4')] (**2**) are orthorhombic space group *Pbca*, a = 1152.8 (3), b = 1471.5 (5), c = 2237.0 (5) pm, Z = 8, and R/R_w = 0.069/0.054. The crystal data for [Fe(NH_3)('N_HS_4')] (**5**) are orthorhombic space group *Pbca*, a = 1107.0 (5), b = 1547.1 (8), c = 2171.9 (9) pm, Z = 8, and R/R_w = 0.040/0.035. σ donor ligands (N_2H_4 or NH_3) cause high-spin states; σ donor, π acceptor ligands (CO, NO, or N_2H_2), however, cause low-spin states of the iron centers. The high-spin 18e$^-$ complexes (L = N_2H_4, NH_3, CH_3OH) exhibit considerably larger Fe–S and Fe–N distances than the low-spin 18e$^-$ compounds (L = CO, $^1/_2$(N_2H_2)). The 19e$^-$ complex [Fe(NO)('N_HS_4')] with low-spin Fe^{II} takes an intermediate position. The correlation between coligands L, spin states, and bond lengths is interpreted in terms of molecular orbital schemes, which also explain why the 18e$^-$ low-spin complexes are highly substitution inert and the 18e$^-$ high-spin complexes are very labile. With regard to the active centers of "Fe-only" nitrogenases, [Fe('N_HS_4')] complexes provide a model. Interrelation of iron spin states, coordination of either σ or σ–π ligands, and substitution lability or inertness may not only support the reduction steps leading from N_2 via N_2H_2 over N_2H_4 to NH_3, but also enable the final step in a catalytic cycle, the substitution of NH_3 by N_2.

Introduction

Coordination compounds of iron are involved in numerous biological systems, e.g., in storage and transportation proteins, electron transferases, and oxidoreductases.[2] The reason for this may be not only the availability and redox activity of iron but also facile spin-state changes of iron centers, as they occur, e.g., in the course of O_2 uptake and release in hemoglobin.[3] Iron is also found in the active centers of nitrogenases, of which now three types are known: Fe/Mo, Fe/V,[4] and the only recently described Fe/Fe nitrogenases which contain exclusively iron.[5] In all nitrogenases the metal coordination spheres predominantly contain sulfur and presumably a few N or O donors.[6] Iron complexes containing biologically relevant donors like thiolate, thioether, or amine ligands in their coordination spheres can consequently be considered model complexes for the active centers of nitrogenases, in particular if they posses binding sites for molecular nitrogen or its reduction products N_2H_2, N_2H_4, and NH_3. In this context, we investigated the chemistry of [Fe(L)('N_HS_4')] complexes. Our aim was to find compounds that potentially reflect structural *and* functional characteristics of the iron centers in Fe/Fe nitrogenase.

Experimental Section

General Methods. Unless noted otherwise, all reactions were carried out under nitrogen at room temperature by using the Schlenk technique. Solvents were dried and distilled under nitrogen before use. Spectra were recorded on the following instruments: Zeiss IMR 16 and Perkin-Elmer 983 infrared spectrometers (solutions in CaF_2 cuvettes with compensation of solvent bands, solids in KBr pellets), Jeol NMR spectrometers JNM-PX 60, JNM-GX 270, and JNM-EX 270, and mass spectrometer Varian MAT 212. Magnetic moments were measured with a Johnson Matthey magnetic susceptibility balance at 295 K. For Mössbauer spectra, all compounds were investigated as powders (ca. 100-mg samples) in polyethylene containers (ϕ = 19 mm). The spectra were recorded under constant acceleration with a multichannel analyzer (Nuclear Data ND 2400) in the multiscaling mode. Calibration was performed with a 25-μm iron foil; isomer shifts δ are referred to metallic iron at 295 K. For measurements at temperatures between 90 and 291 K a nitrogen thermostat was used, and for measurements at 4 K a helium thermostat was used.

[Fe(CO)('N_HS_4')],[7] [Fe(NO)('N_HS_4')],[8] and [μ-N_2H_2{Fe('N_HS_4')}$_2$][9] were prepared as described in the literature. Hydrazine (ca. 93%) was

* To whom correspondence should be addressed.
† Institut für Anorganische Chemie.
‡ Physikalisches Institut.

(1) Part 87: Sellmann, D.; Grasser, F.; Knoch, F.; Moll, M. *Inorg. Chim. Acta* **1992**, *195*, 25.
(2) Sigel, H. *Metal Ions in Biological Systems*; Marcel Dekker: New York, 1978; Vol. 7.
(3) a) Perutz, M. F. *Nature* **1972**, *237*, 495. b) Perutz, M. F. *Nature* **1970**, *228*, 726. c) Hughes, M. N. *The Inorganic Chemistry of Biological Processes*; Wiley: New York, 1981.
(4) a) Lowe, D. J.; Thorneley, R. N. F.; Smith, B. E. In *Metalloproteins Part 1, Metal Proteins with Redox Roles*; Harrison, P., Ed.; Verlag Chemie: Weinheim, 1985. b) Bergersen, F. J.; Postgate, J. R. *A Century of Nitrogen Fixation Research*; The Royal Society: London, 1987.
(5) Chisnell, J. R.; Premakumar, R.; Bishop, P. E. *J. Bacteriol.* **1988**, *170*, 27.
(6) Hoover, T. R.; Imperial, J.; Ludden, P. W.; Shah, V. K. *Biochemistry* **1989**, *28*, 2768.
(7) Sellmann, D.; Kunstmann, H.; Knoch, F.; Moll, M. *Inorg. Chem.* **1988**, *27*, 4183.
(8) Sellmann, D.; Kunstmann, H.; Moll, M.; Knoch, F. *Inorg. Chim. Acta* **1988**, *154*, 157.
(9) Sellmann, D.; Soglowek, W.; Knoch, F.; Moll, M. *Angew. Chem.* **1989**, *101*, 1244; *Angew. Chem., Int. Ed. Engl.* **1989**, *28*, 1271.

0020-1669/92/1331-3711$03.00/0

Table I. Selected Crystallographic Data of $[Fe(N_2H_4)('N_HS_4')]$ (**1a**), $[Fe(CH_3OH)('N_HS_4')]$ (**2**), and $[Fe(NH_3)('N_HS_4')]$ (**5**)

formula	$C_{16}H_{21}N_3S_4Fe$	$C_{17}H_{21}NS_4OFe$	$C_{16}H_{20}N_2S_4Fe$
M_r	439.47	439.47	424.45
space group	*Pbca*	*Pbca*	*Pbca*
a, pm	1102.1 (7)	1152.8 (3)	1107.0 (5)
b, pm	1567.2 (8)	1471.5 (5)	1547.1 (8)
c, pm	2206.6 (14)	2237.0 (5)	2171.9 (9)
cell volume, pm³	3811 (3) × 10⁶	3795 (2) × 10⁶	3719 (3) × 10⁶
molecules/unit cell	8	8	8
δ_{calc}, g/cm³	1.53	1.54	1.52
μ, cm⁻¹	12.1	12.2	12.4
radiation Mo Kα wavelength, pm	71.073	71.073	71.073
temp of measurement, K	293	200	200
R/R_w, %	4.6/4.6	6.9/5.4	4.0/3.5
reflections, collected	3851	4493	3562
reflections, independent	3381	3113	2913
reflections, observed	2215	1835	2607
σ-criterion	$F > 4\sigma(F)$	$F > 6\sigma(F)$	$F > 4\sigma(F)$
parameters, refined	218	218	209

obtained by 2-fold distillation of $N_2H_4 \cdot H_2O$ over solid KOH.[10] *Caution: Hydrazine may cause cancer and explode when heated under standard pressure. It should be handled only in a hood and distilled at reduced pressure behind a safety pane.*

X-ray Structure Analyses of $[Fe(N_2H_4)('N_HS_4')]$ (1a), $[Fe(CH_3OH)('N_HS_4')]$ (2), and $[Fe(NH_3)('N_HS_4')]$ (5). Single crystals of $[Fe(N_2H_4)('N_HS_4')]$ (**1a**), $[Fe(CH_3OH)('N_HS_4')]$ (**2**), and $[Fe(NH_3)('N_HS_4')]$ (**5**) were grown in Schlenk tubes that contained saturated solutions of **1a** in $THF/CH_3OH/N_2H_4$ (1:1:0.02), **2** in CH_3OH, or **5** in CH_3OH (NH_3-saturated). The Schlenk tubes were plugged by rubber stoppers and kept at ambient temperatures for several weeks. Precipitating single crystals were removed, sealed in glass capillaries, and mounted on a Siemens P4 (**1a**) or a Nicolet R3m/V diffractometer (**2**, **5**). Corrections for absorption were not applied. The structures were solved by direct methods (SHELXTL-PLUS). Non-hydrogen atoms were refined with anisotropic thermal parameters, aromatic H atoms were placed at calculated positions and refined as rigid groups, and hydrogen atoms of the methylene groups of $'N_HS_4'^{2-}$ and of the amine, methyl, and hydroxyl groups of the coligands were placed in ideal tetrahedral positions and were allowed to rotate around their central atom during refinement. Hydrogen atoms were refined with common isotropic thermal parameters.

Table I lists selected crystallographic data, and Table II lists fractional atomic coordinates and equivalent thermal parameters.

Preparation of Compounds. $[Fe(N_2H_4)('N_HS_4')]$ (1a) from $[Fe(CO)('N_HS_4')]$. A mixture of N_2H_4 (1.0 mL, ca. 30 mmol) and $[Fe(CO)('N_HS_4')]$ (2.99 g, 6.86 mmol) in 130 mL of THF was kept boiling for 68 h. An additional 0.5 mL of N_2H_4 was added to the boiling solution after 28 and 53 h, respectively. The resulting yellow-brown suspension was reduced in volume to one-third, and the yellow-brown precipitate was collected, washed with 10 mL of THF, and dried in vacuo. Yield: 2.63 g (88%). Anal. Calcd for $C_{16}H_{21}N_3S_4Fe$ (M_r = 439.5): C, 43.73; H, 4.82; N, 9.56. Found: C, 43.58; H, 5.02; N, 9.30. FD MS (*m*/*z*): 439 [M⁺]. IR (KBr, cm⁻¹): 3310 w, 3300 sh, 3250 w, 3240 sh, 3120 w (ν_{NH}), 1605 m, 1585 w (δ_{NH}).

$[Fe(N_2H_4)('N_HS_4')]$ (1a) from $[Fe(CH_3OH)('N_HS_4')]$ (2). A yellow-green suspension of $[Fe(CH_3OH)('N_HS_4')]$ (400 mg, 0.91 mmol) in 10 mL of THF was combined with 0.5 mL (ca. 15 mmol) of N_2H_4 and stirred for 16 h. The resulting light brown solid was collected, washed with 12 mL of CH_3OH, and dried in vacuo. Yield: 370 mg (92%). Anal. Calcd for $C_{16}H_{21}N_3S_4Fe$ (M_r = 439.5): C, 43.73; H, 4.82; N, 9.56. Found: C, 43.59; H, 5.45; N, 9.28.

$[Fe(N_2H_4)('N_HS_4')]$ (1b). A red solution of N_2H_4 (1.0 mL, ca. 30 mmol) and $[Fe(CO)('N_HS_4')]$ (1.60 g, 3.68 mmol) in 50 mL of THF was kept boiling for 18 h only, and no extra N_2H_4 was added in the course of the reaction. The resulting brown precipitate was collected, washed with 10 mL of THF, and dried in vacuo. Bubbling CO through the filtrate allowed recovery of 350 mg of $[Fe(CO)('N_HS_4')]$. Yield: 900 mg (71%). Anal. Calcd for $C_{16}H_{21}N_3S_4Fe$ (M_r = 439.5): C, 43.73; H, 4.82; N, 9.56. Found: C, 44.04; H, 5.21; N, 9.56. FD MS (*m*/*z*): 439 [M⁺]. IR (KBr, cm⁻¹): 3280 w, 3250 vw, 3220 vw, 3140 w (ν_{NH}), 1610 m, 1585 m (δ_{NH}).

$[Fe(CO)('N_HS_4')]$ from $[Fe(CH_3OH)('N_HS_4')]$ (2). CO was bubbled through a solution of $[Fe(CH_3OH)('N_HS_4')]$ (280 mg, 0.64 mmol) in 10 mL of DMF for 60 s. The color of the solution changed immediately from yellow to red. The solvent was removed and the red residue recrystallized at −30 °C from CH_2Cl_2 (10 mL) which was covered with a layer of CH_3OH (10 mL). Yield: 170 mg (61%). Anal. Calcd for $C_{17}H_{17}NS_4OFe$ (M_r = 435.4): C, 46.89; H, 3.94; N, 3.22. Found: C, 47.12; H, 4.09; N, 3.10.

$[Fe(CO)('N_HS_4')]$ from $[Fe(N_2H_4)('N_HS_4')]$ (1a). When CO was bubbled through a solution of $[Fe(N_2H_4)('N_HS_4')]$ (**1a**) (150 mg, 0.34 mmol) in 10 mL of DMF for 15 min, the color of the solution immediately changed from yellow to red. The solvent was removed and the red residue recrystallized from CH_2Cl_2 which was covered with a layer of CH_3OH. Yield: 120 mg (81%). The resulting red crystals were identified as $[Fe(CO)('N_HS_4')]$ by their KBr IR spectrum.

$[Fe(CH_3OH)('N_HS_4')]$ (2). $[Fe(N_2H_4)('N_HS_4')]$ (1.15 g, 2.61 mmol) was digested with CH_3OH for 14 h in an extraction frit,[11] and the remaining yellow-green solid was dried in vacuo. Yield: 880 mg (76%). Anal. Calcd for $C_{17}H_{21}NOS_4Fe$ (M_r = 439.5): C, 46.46; H, 4.82; N, 3.19. Found: C, 46.35; H, 4.94; N, 3.19. FD MS (*m*/*z*): 439 [M⁺]. IR (KBr, cm⁻¹): 3300 w (ν_{NH}), 3120 w (ν_{OH}), 1005 s (ν_{CO}).

$[Fe(THF)('N_HS_4')]$ (3). A 5-mL portion of H_2O was added to a suspension of $[Fe(CH_3OH)('N_HS_4')]$ (**2**) (300 mg, 0.68 mmol) in 15 mL of THF. Immediately a clear orange solution resulted, which was stirred for 20 min. The solvent was removed and the resulting green-yellow powder dried in vacuo. Yield: 300 mg (92%). Anal. Calcd for $C_{20}H_{25}NS_4OFe$ (M_r = 479.5): C, 50.09; H, 5.26; N, 2.92. Found: C, 49.74; H, 5.25; N, 2.91. FD MS (*m*/*z*): 479 [M⁺]. IR (KBr, cm⁻¹): 3100 w (ν_{NH}), 2910 w, 2860 w (ν_{CH}).

$[Fe(py)('N_HS_4')]$ (4). $[Fe(CH_3OH)('N_HS_4')]$ (**2**) (220 mg, 0.50 mmol) was dissolved in 50 mL of pyridine at 50 °C. When the solution was cooled to room temperature, yellow microcrystals precipitated, which were collected, washed with 5 mL of pyridine, and dried in vacuo. Yield: 210 mg (86%). Anal. Calcd for $C_{21}H_{22}N_2S_4Fe$ (M_r = 486.5): C, 51.84; H, 4.56; N, 5.76. Found: C, 51.47; H, 4.53; N, 5.94. FD MS (*m*/*z*): 407 [M⁺ − py]. IR (KBr, cm⁻¹): 3250 m (ν_{NH}), 3040 w (ν_{CH}), 745 vs (δ_{CH}).

$[Fe(NH_3)('N_HS_4')]$ (5). Through a suspension of $[Fe(CH_3OH)('N_HS_4')]$ (**2**) (460 mg, 1.05 mmol) in 20 mL of H_2O, gaseous NH_3 was bubbled for 2.5 h, and the reaction mixture was stirred under an atmosphere of NH_3 for another 15 h. The resulting yellow-green solid was collected and dried in vacuo. Yield: 445 mg (100%). Anal. Calcd for $C_{16}H_{20}N_2S_4Fe$ (M_r = 424.5): C, 45.28; H, 4.75; N, 6.60. Found: C, 44.90; H, 4.90; N, 6.09. FD MS (*m*/*z*): 407 [M⁺ − NH_3]. IR (KBr, cm⁻¹): 3360 w, 3300 w, 3220 w, 3140 w (ν_{NH}), 1605 m, 1590 m (δ_{NH}).

$[Fe(NHCH_3NH_2)('N_HS_4')]$ (6). $NHCH_3NH_2$ (0.6 mL, 11.4 mmol) was added to a suspension of $[Fe(CH_3OH)('N_HS_4')]$ (**2**) (430 mg, 0.98 mmol) in 25 mL of THF/hexane (4:1). The mixture was stirred for 15 h, and the resulting light yellow solid was collected, washed with 15 mL of hexane, and dried in vacuo. Yield: 305 mg (69%). Anal. Calcd for $C_{17}H_{23}N_3S_4Fe$ (M_r = 453.5): C, 45.03; H, 5.11; N, 9.27. Found: C, 45.06; H, 5.18; N, 8.89. FD MS (*m*/*z*): 407 [M⁺ − $NHCH_3NH_2$]. IR (KBr, cm⁻¹): 3240 w, 3190 w, 3140 w, 3110 w (ν_{NH}), 1590 (δ_{NH}).

$[Fe(P(OPh)_3)('N_HS_4')]$ (7). $P(OPh)_3$ (0.12 mL, 0.45 mmol) was added to a suspension of $[Fe(CH_3OH)('N_HS_4')]$ (200 mg, 0.45 mmol) in 20 mL of CH_2Cl_2. A red-green solution resulted that was stirred for 4 h. The solvent was evaporated, and the remaining residue was digested with 20 mL of CH_3OH for 7 h, collected, washed with 24 mL of CH_3OH, and dried in vacuo. Yield: 220 mg (68%). Anal. Calcd for $C_{34}H_{32}NS_4O_3PFe$ (M_r = 717.7): C, 56.90; H, 4.49; N, 1.95. Found: C, 56.59; H, 4.34; N, 1.68. FD MS (*m*/*z*): 717 [M⁺]. IR (KBr, cm⁻¹): 3180 w (ν_{NH}), 1235 s, 1225 s, 1200 s, 1180 s, 900 s. ^1H NMR (δ, ppm; CD_2Cl_2): 6.5–7.8 (m, 23 H), 1.4–3.8 (m, 9 H). When recrystallized from CH_2Cl_2 which was covered with a layer of ether, the product was obtained as red crystals.

$[Fe(P(OCH_3)_3)('N_HS_4')]$ (8). $P(OCH_3)_3$ (0.184 mL, 1.56 mmol) was added to a suspension of $[Fe(CH_3OH)('N_HS_4')]$ (690 mg, 1.56 mmol) in 40 mL of CH_2Cl_2. A green solution resulted that was stirred for 3 h. The solvent was evaporated, and the remaining residue was digested with 20 mL of hexane for 2 h, collected, and dried in vacuo. Recrystallization from DMF (30 mL) which was layered with CH_3OH (20 mL) yielded deep red crystals, which were collected, washed with 15 mL of CH_3OH, and dried in vacuo. Yield: 600 mg (72%). Anal. Calcd for $C_{19}H_{26}NS_4O_3PFe$ (M_r = 531.5): C, 42.94; H, 4.93; N, 2.64. Found: C, 43.12; H, 5.02; N, 2.50. FD MS (*m*/*z*): 469 [M⁺ − $2OCH_3$], 407 [M⁺ − $P(OCH_3)_3$]. IR (KBr, cm⁻¹): 3240 m (ν_{NH}), 1090 m, 1070 m, 1040 s, 1015 s. ^1H NMR (δ, ppm; $CDCl_3$): 6.8–8.2 (m, 8 H); 2.2–3.9 (m, 9 H); 3.3 (d, 9 H).

(10) Bock, H. *Z. Anorg. Allg. Chem.* **1958**, *293*, 265.

(11) Brauer, G. *Handbuch der präparativen Anorganischen Chemie*; Verlag Enke: Stuttgart, 1981.

Table II. Fractional Atomic Coordinates ($\times 10^4$) and Isotropic Thermal Parameters ($pm^2 \times 10^{-1}$) of $[Fe(N_2H_4)('N_HS_4')]$ (**1a**), $[Fe(CH_3OH)('N_HS_4')]$ (**2**), and $[Fe(NH_3)('N_HS_4')]$ (**5**)

	x	y	z	$U(eq)^a$		x	y	z	$U(eq)^a$
				$[Fe(N_2H_4)('N_HS_4')]$ (**1a**)					
Fe(1)	2328 (1)	1571 (1)	4781 (1)	25 (1)	C(11)	4432 (7)	712 (5)	6542 (3)	33 (2)
N(2)	975 (5)	2378 (4)	5231 (3)	31 (2)	C(10)	3597 (7)	828 (5)	6072 (3)	29 (2)
N(3)	1361 (8)	2901 (5)	5731 (3)	53 (3)	C(25)	1169 (7)	2127 (5)	3365 (3)	29 (2)
S(1)	3844 (2)	1661 (1)	5547 (1)	36 (1)	C(24)	437 (8)	2207 (5)	2859 (3)	37 (3)
S(2)	1491 (2)	347 (1)	5459 (1)	30 (1)	C(23)	771 (9)	2726 (6)	2394 (4)	45 (3)
S(3)	3204 (2)	2552 (1)	4068 (1)	33 (1)	C(22)	1828 (9)	3194 (6)	2435 (4)	45 (3)
S(4)	678 (2)	1399 (1)	3946 (1)	29 (1)	C(21)	2539 (8)	3135 (5)	2941 (4)	38 (3)
N(1)	3111 (6)	432 (4)	4295 (3)	32 (2)	C(20)	2245 (7)	2592 (5)	3428 (3)	30 (2)
C(15)	2609 (7)	272 (4)	6049 (3)	26 (2)	C(16)	1948 (8)	−544 (5)	4987 (3)	35 (3)
C(14)	2460 (8)	−366 (5)	6481 (3)	37 (3)	C(17)	3139 (8)	−364 (5)	4655 (4)	40 (3)
C(13)	3294 (9)	−473 (6)	6936 (4)	46 (3)	C(26)	1264 (7)	397 (5)	3636 (3)	34 (3)
C(12)	4295 (8)	64 (6)	6963 (4)	43 (3)	C(27)	2632 (8)	342 (5)	3668 (3)	38 (3)
				$[Fe(CH_3OH)('N_HS_4')]$ (**2**)					
Fe(1)	2249 (1)	3462 (1)	379 (1)	19 (1)	C(24)	2501 (8)	5284 (6)	1413 (3)	29 (3)
S(1)	3046 (2)	2528 (2)	1149 (1)	25 (1)	C(23)	3337 (9)	5346 (7)	1842 (4)	33 (3)
S(2)	602 (2)	3735 (1)	1137 (1)	24 (1)	C(22)	4276 (8)	4766 (6)	1817 (4)	33 (3)
S(3)	1513 (2)	4655 (1)	−378 (1)	24 (1)	C(21)	4407 (7)	4146 (6)	1366 (4)	29 (3)
S(4)	3788 (2)	3286 (1)	−323 (1)	27 (1)	C(20)	3587 (7)	4074 (6)	−904 (3)	21 (2)
C(15)	1004 (7)	3010 (6)	1749 (4)	23 (2)	N(1)	2950 (6)	4700 (4)	799 (3)	22 (2)
C(14)	228 (8)	2931 (7)	2224 (4)	29 (3)	C(16)	1146 (8)	4818 (6)	1416 (4)	30 (3)
C(13)	473 (8)	2419 (7)	2706 (4)	34 (3)	C(17)	2458 (8)	4883 (6)	1403 (4)	31 (3)
C(12)	1528 (9)	1940 (6)	2727 (4)	35 (3)	C(26)	1918 (8)	5659 (6)	43 (4)	23 (2)
C(11)	2292 (8)	2007 (6)	2255 (3)	26 (2)	C(27)	3028 (7)	5512 (6)	397 (4)	29 (2)
C(10)	2047 (7)	2540 (5)	1745 (3)	21 (2)	C(1)	1054 (8)	2369 (8)	−683 (4)	38 (3)
C(25)	2631 (7)	4662 (5)	−929 (3)	21 (2)	O(1)	1150 (5)	2528 (4)	−58 (2)	26 (2)
				$[Fe(NH_3)('N_HS_4')]$ (**5**)					
Fe(1)	2295 (1)	3403 (1)	236 (1)	21 (1)	C(24)	2515 (4)	5420 (3)	−1446 (2)	33 (1)
S(1)	3182 (1)	2425 (1)	962 (1)	27 (1)	C(23)	3392 (4)	5558 (3)	−1890 (2)	39 (2)
S(2)	625 (1)	3550 (1)	1063 (1)	25 (1)	C(22)	4383 (4)	5014 (3)	−1914 (2)	35 (2)
S(3)	1495 (1)	4644 (1)	−450 (1)	23 (1)	C(21)	4499 (4)	4334 (3)	−1502 (2)	26 (1)
S(4)	3886 (1)	3349 (1)	−510 (1)	28 (1)	C(20)	3649 (3)	4192 (2)	−1034 (2)	21 (1)
C(15)	1108 (3)	2823 (2)	1647 (2)	23 (1)	N(1)	3041 (3)	4544 (2)	747 (1)	25 (1)
C(14)	378 (4)	2737 (3)	2166 (2)	31 (1)	C(16)	1164 (3)	4556 (3)	1391 (2)	29 (1)
C(13)	713 (4)	2214 (3)	2652 (2)	36 (2)	C(17)	2542 (4)	4633 (3)	1381 (2)	27 (1)
C(12)	1789 (4)	1767 (3)	2614 (2)	37 (2)	C(26)	1901 (4)	5538 (2)	48 (2)	28 (1)
C(11)	2514 (4)	1833 (3)	2099 (2)	32 (1)	C(27)	3088 (3)	5371 (2)	389 (2)	27 (1)
C(10)	2206 (4)	2367 (2)	1602 (2)	25 (1)	N(2)	1121 (3)	2538 (2)	−292 (1)	31 (1)
C(25)	2647 (4)	4751 (2)	−1018 (2)	24 (1)					

[a] Equivalent isotropic U defined as one-third of the trace of the orthogonalized U_{ij} tensor.

$[Fe('N_HS_4')]_x$ (9). A suspension of $[Fe(CH_3OH)('N_HS_4')]$ (**2**) (270 mg, 0.61 mmol) in 15 mL of CH_2Cl_2 was stirred for 18 h. The resulting yellow solid was collected, washed with 10 mL of CH_2Cl_2, and dried in vacuo. Yield: 230 mg (93%). Anal. Calcd for $C_{16}H_{17}NS_4Fe$ (M_r = 407.4): C, 47.17; H, 4.21; N, 3.44. Found: C, 47.16; H, 4.29; N, 3.26. FD MS (m/z): 407 [M^+, x = 1]; 814 [M^+, x = 2]. IR (KBr, cm^{-1}): 3250 m, 3120 m (ν_{NH}).

$['N_HS_4'\text{-}H_2]\cdot HCl$ (10). Aqueous HCl (37%, 1.40 mL, 16.8 mmol) was added to a solution of $[Fe(CO)('N_HS_4')]$ (2.00 g, 4.60 mmol) in 120 mL of CH_2Cl_2. When the mixture was boiled for 3 h, its color changed from red to yellow. After addition of dry Na_2SO_4 (5 g) and 1 h of additional stirring, the solution was filtered and the remaining Na_2SO_4 washed with 40 mL of CH_2Cl_2. The combined filtrates were evaporated, yielding a white residue that was digested with 20 mL of hexane for 3 h, collected, washed with another 20 mL of hexane, and dried in vacuo. Yield: 1.50 g (84%). Anal. Calcd for $C_{16}H_{20}NS_4Cl$ (M_r = 390.1): C, 49.27; H, 5.17; N, 3.59. Found: C, 49.41; H, 5.19; N, 3.36. EI MS (m/z): 354 [M^+ − Cl]. IR (KBr, cm^{-1}): 2740 s, 2400 s (ν_{SH}). ^1H NMR (δ, ppm; CD_2Cl_2): 10.00 (s, 2 H); 6.85–7.15 (m, 8 H); 4.30 (s, 2 H); 2.9–3.6 (m, 8 H).

Results

Synthesis, Characterization, and Reactions of $[Fe(L)('N_HS_4')]$ Complexes. Reaction of diamagnetic $[Fe(CO)('N_HS_4')]$ with hydrazine according to eq 1 gave optimized yields of $[Fe(N_2H_4)('N_HS_4')]$[7] (**1**) up to 80%.

Dependent on the reaction conditions (cf. exp. section), the hydrazine complex forms as either **1a** or **1b**. With respect to elemental analysis, mass spectroscopy (m/z = 439, M^+), Mössbauer spectroscopy (**1a**, δ = 0.930 mm/s, ΔE_Q = 2.999 mm/s, 4.2 K; **1b**, δ = 0.914 mm/s, ΔE_Q = 2.940 mm/s, 90 K),

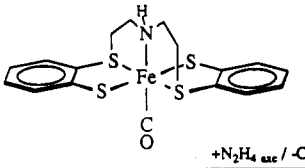

$\xrightarrow[68\ h\ /\ 66°C]{+N_2H_4\ exc\ /\ -CO/\ THF}$ $[Fe(N_2H_4)('N_HS_4')]$ (1) (1)

and magnetism (**1a**, μ_{eff} = 4.98 μ_B; **1b**, μ_{eff} = 5.02 μ_B), **1a** and **1b** show practically identical properties. The magnetic moments correspond to four unpaired electrons of Fe^{II} high-spin centers in both cases. Both complexes yielded also ^1H NMR spectra that showed only extremely broad, unresolved signals in the region from −30 to +120 ppm which could not be assigned. The same holds for all paramagnetic high-spin complexes described here.

1a and **1b**, however, can be distinguished clearly by their KBr IR spectra that show distinctly different absorptions in the ν_{NH} and δ_{NH} regions (Figure 1).

A complete structural characterization was possible for **1a**, whose molecular structure was elucidated by X-ray structure analysis. It is schematically shown in Figure 2a and represents the meso isomer[7] of $[Fe(N_2H_4)('N_HS_4')]$ in which both thiolate S atoms coordinate the iron center in cis positions.

Due to the lack of suitable single crystals, X-ray structure analysis of **1b** was not possible so far. Because of its IR spectrum, **1b** has to have a different structure that is possibly the racemic stereoisomer with trans thiolate donors of Figure 2b.

1a and **1b** are soluble in DMF and DMSO and only sparingly soluble in THF. In contact with air, these solutions first become

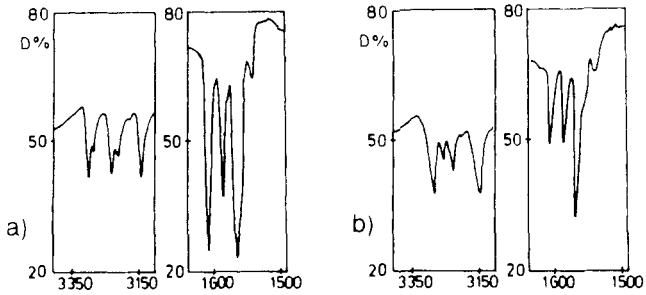

Figure 1. ν_{NH} and δ_{NH} regions of the KBr IR spectra of (a) **1a** and (b) **1b** (transmission (%) vs ν (cm^{-1})).

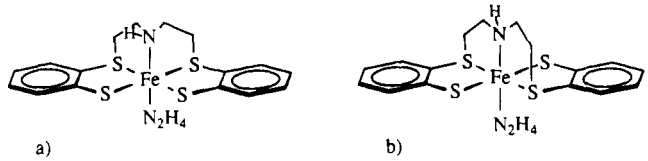

Figure 2. Schematic drawings of structural isomers of $[Fe(N_2H_4)('N_HS_4')]$: (a) molecular structure of **1a**, (b) proposed structure of **1b**.

deep blue and after a few minutes yellow-brown. Simultaneously a flocculent brown solid precipitates. As reported previously, the dinuclear diazene complex $[\mu\text{-}N_2H_2\{Fe('N_HS_4')\}_2]$ can be isolated from the blue solutions at −60 °C.[9]

When digested with methanol, **1a** and **1b** yield the CH_3OH complex $[Fe(CH_3OH)('N_HS_4')]$ (**2**) (eq 2).

$$\textbf{1a or 1b} \xrightarrow[30°C/14h]{CH_3OH/-N_2H_4} [Fe(CH_3OH)('N_HS_4')]\ (\textbf{2}) \quad (2)$$

The KBr IR spectrum of **2** shows a broad ν_{OH} absorption at 3120 cm^{-1} and a sharp ν_{CO} absorption at 1005 cm^{-1} in addition to the typical $[Fe('N_HS_4')]$ bands. **2** is paramagnetic (μ_{eff} = 4.88 μ_B) like **1a** and **1b**, but in contrast to those, only one isomer was observed and was characterized as *meso*-**2** by X-ray structure analysis.

The CH_3OH ligand in **2** is very labile. This makes **2** an ideal starting compound for syntheses of other $[Fe(L)('N_HS_4')]$ complexes according to eq 3.

$$[Fe(CH_3OH)('N_HS_4')]\ (\textbf{2}) + L \rightarrow [Fe(L)('N_HS_4')] + CH_3OH \quad (3)$$

L = THF (**3**), py (**4**), NH_3 (**5**), $NHCH_3NH_2$ (**6**), $P(OPh)_3$ (**7**), $P(OMe)_3$ (**8**), CO

$[Fe(THF)('N_HS_4')]$ (**3**) was obtained by stirring **2** in a mixture of THF and H_2O. The presence of water strongly accelerated the reaction, possibly because it improves the solvation of decoordinated CH_3OH. **3** is a green-yellow, paramagnetic (μ_{eff} = 4.92 μ_B) powder which is extremely air sensitive.

$[Fe(NH_3)('N_HS_4')]$ (**5**) formed when gaseous NH_3 was bubbled through a suspension of **2** in water. **5** forms light yellow crystals and is also paramagnetic. Susceptibility measurements, however, repeatedly gave anomalous high μ_{eff} values of 10–13 μ_B. Because the starting material **2** possesses a normal μ_{eff} of ca. 5 μ_B and the molecular structures of **2** and **5** are fully analogous, such high μ_{eff} values cannot be explained and are possibly due to impurities, e.g., small amounts of metallic iron.

The high-spin complexes $[Fe(py)('N_HS_4')]$ (**4**) (μ_{eff} = 4.72 μ_B) and $[Fe(NHCH_3NH_2)('N_HS_4')]$ (**6**) (μ_{eff} = 4.72 μ_B) formed when **2** was dissolved in pyridine or **2** was reacted with $NHCH_3NH_2$ in a THF/hexane suspension, respectively. These reactions can be carried out also in CH_3OH, then, however, **2** is always formed as a byproduct. In spite of several attempts, neither the aquo complex $[Fe(H_2O)('N_HS_4')]$ nor thioether complex $[Fe(SR\text{-}R')('N_HS_4')]$ (e.g., R = CH_3, R′ = Ph) could be obtained.

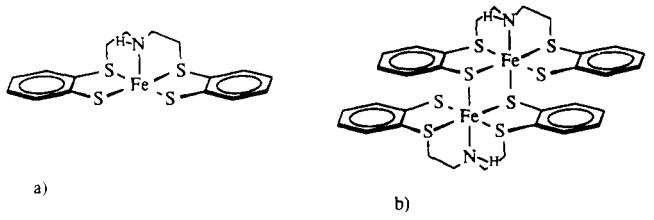

Figure 3. Proposed molecular structures of $[Fe('N_HS_4')]_x$ for (a) x = 1 and (b) x = 2.

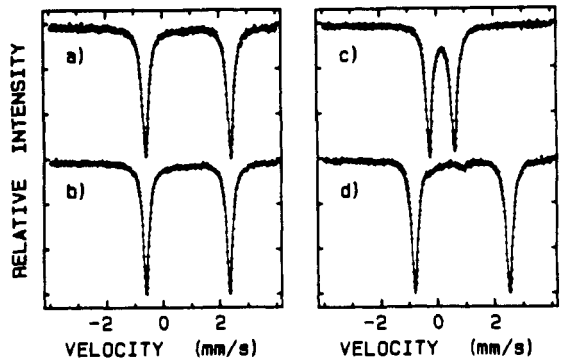

Figure 4. Mössbauer spectra of (a) $[Fe(N_2H_4)('N_HS_4')]$ (**1a**; 4 K), (b) $[Fe(N_2H_4)('N_HS_4')]$ (**1b**; 101 K), (c) $[Fe(CO)('N_HS_4')]$ (101 K), and (d) $[Fe('N_HS_4')]_x$ (**9**; 101 K).

While **2** always yields paramagnetic 18e⁻ complexes when reacted with σ ligands, its reactions with σ–π ligands very rapidly yield diamagnetic 18e⁻ complexes, e.g., $[Fe(P(OR)_3)('N_HS_4')]$ with phosphite donors (R = Ph (**7**), Me (**8**)) or $[Fe(CO)('N_HS_4')]$ with CO.

The coligand CH_3OH in $[Fe(CH_3OH)('N_HS_4')]$ (**2**) is so loosely bound that it splits off readily when a suspension of **2** is stirred in noncoordinating solvents such as CH_2Cl_2 or toluene (eq 4).

$$x[Fe(CH_3OH)('N_HS_4')]\ (\textbf{2}) \xrightarrow[18h]{CH_2Cl_2/20°C} [Fe('N_HS_4')]_x\ (\textbf{9}) + xCH_3OH \quad (4)$$

In the course of this reaction, first a nearly clear, deep yellow solution forms, from which a yellow powder precipitates within a few minutes. It was characterized as the unsolvated $[Fe('N_HS_4')]_x$ (**9**), but it could not yet be decided whether **9** is mono- (Figure 3a) or dinuclear (Figure 3b). The observed course of the reaction indicates that first the coordinatively unsaturated fragment $[Fe('N_HS_4')]$ is formed, which subsequently dimerizes to give the dinuclear $[Fe('N_HS_4')]_2$ complex.

Solubility, magnetism, IR and mass spectra, and the Mössbauer spectrum of the yellow powder are consistent with formation of dinuclear $[Fe('N_HS_4')]_2$. The magnetic moment μ_{eff} = 4.3 μ_B per iron center of **9** is distinctively smaller than those of the mononuclear complexes **1a–4** (μ_{eff} = ca. 5 μ_B). This could be due to spin coupling as found, e.g., in $[Fe('S_2')_2]_2^{2-}$.[12] Formation of the dinuclear complex $[Fe('N_HS_4')]_2$ can also be deduced from the mass spectrum of **9** that always shows the signal of $[Fe('N_HS_4')]_2^+$ (m/z = 814) in addition to the ion of mononuclear $[Fe('N_HS_4')]^+$ (m/z = 407).

In order to gain further information about the coordination geometry and spin state of $[Fe('N_HS_4')]_x$, Mössbauer spectra of $[Fe('N_HS_4')]_x$ (**9**) and, for reasons of comparison, low-spin $[Fe(CO)('N_HS_4')]$ as well as high-spin $[Fe(N_2H_4)('N_HS_4')]$, **1a** and **1b**, were recorded. The spectra are shown in Figure 4; Table III summarizes selected data.

The zero-field spectra of $[Fe(CO)('N_HS_4')]$, $[Fe(N_2H_4)('N_HS_4')]$ (**1a** and **1b**), and $[Fe('N_HS_4')]_x$ (**9**) show symmetrical

(12) Sellmann, D.; Geck, M.; Moll, M. *J. Am. Chem. Soc.* **1991**, *113*, 5259.

Table III. Mössbauer Isomer Shifts (δ),[a] Quadrupole Splittings (ΔE_Q), and Line Widths (Γ) of [Fe(CO)('N_HS_4')], [Fe(N_2H_4)('N_HS_4')] (**1a** and **1b**), [Fe('N_HS_4')]$_x$ (**9**), and [Fe('S_4')(TMEDA)][b]

complex	T, K	δ, mm/s	ΔE_Q, mm/s	Γ, mm/s
[Fe(CO)('N_HS_4')]	291	0.134	0.842	0.244, 0.279
	101	0.210	0.874	0.260, 0.278
[Fe(N_2H_4)('N_HS_4')] (**1a**)	4.2	0.930	2.999	0.276, 0.270
[Fe(N_2H_4)('N_HS_4')] (**1b**)	291	0.792	2.961	0.244, 0.237
	101	0.908	2.942	0.245, 0.242
	90	0.914	2.940	0.245, 0.239
[Fe('N_HS_4')]$_x$ (**9**)	291	0.782	3.299	0.271
	150	0.871	3.312	0.271
	101	0.898	3.310	0.274
[Fe('S_4')(TMEDA)]	295	0.860	2.360	

[a] Referred to metallic iron at room temperature. [b] Cf. ref 14; 'S_4'$^{2-}$ = dianion of 1,2-bis[(2-mercaptophenyl)thio]ethane.

quadrupole doublets at all temperatures. The isomer shift and quadrupole splitting of [Fe(CO)('N_HS_4')] are typical of low-spin six-coordinate Fe^{II} compounds,[13,14] and the corresponding parameters of [Fe(N_2H_4)('N_HS_4')] (**1a** and **1b**) are typical of high-spin six-coordinate Fe^{II} complexes and compare well with the data of related compounds, e.g., [Fe('S_4')(TMEDA)].[14]

The isomer shift of [Fe('N_HS_4')]$_x$ (**9**) is also typical of high-spin Fe^{II} complexes and corresponds to the magnetic moment μ_{eff} = 4.3 μ_B. The quadrupole splitting that sensitively depends on the coordination geometry of the iron center is comparable to those of six-coordinate complexes like [Fe(N_2H_4)('N_HS_4')] (**1a** and **1b**) or [Fe('S_4')(TMEDA)]. In conclusion, the Mössbauer results suggest for [Fe('N_HS_4')]$_x$ six-coordinate iron centers that form when two [Fe('N_HS_4')] fragments dimerize and a bridging thiolate donor occupies the sixth coordination site in the [Fe('N_HS_4')] fragments according to Figure 3b.

Temperature-dependent measurements of **1a**, **1b**, and [Fe('N_HS_4')]$_x$ (**9**) indicated a normal behavior of the isomer shifts and did not yield any evidence for spin-state changes as found, e.g., for [Fe(phen)$_2$(NCS)$_2$][15] at 170 K.

The substitution lability of coligand L in all high-spin [Fe(L)('N_HS_4')] complexes renders possible reversible interconversions of high-spin complexes under mild conditions, e.g., according to eq 5.

$$[Fe(CH_3OH)('N_HS_4')]\ (\mathbf{2}) + N_2H_4 \underset{30°C/14h}{\overset{20°C/16h}{\rightleftarrows}} [Fe(N_2H_4)('N_HS_4')]\ (\mathbf{1}) + CH_3OH \quad (5)$$

The reaction of high-spin [Fe(L)('N_HS_4')] complexes yielding low-spin derivatives, e.g., according to eq 6, also takes place at room temperature; the reverse reaction, however, requires drastic conditions and long reaction times.

$$[Fe(N_2H_4)('N_HS_4')]\ (\mathbf{1a}) \underset{+N_2H_4/-CO/66°C/68\ h}{\overset{+CO/-N_2H_4/20°C/2min}{\rightleftarrows}} [Fe(CO)('N_HS_4')] \quad (6)$$

In contrast to the fairly air stable low-spin derivatives, the high-spin compounds all are highly sensitive to oxidation. For example, the yellow crystals of [Fe(THF)('N_HS_4')] (**3**) turn black within a few seconds when air is admitted.

In analogy to the smooth reactions according to eq 5, the synthesis of the dinuclear hydrazine complex [μ-N_2H_4-{Fe('N_HS_4')}$_2$] was attempted according to eqs 7 and 8.

[μ-N_2H_4{Fe('N_HS_4')}$_2$] was detected in the raw product by FD mass spectroscopy, but it could not be isolated in the pure state. Either [Fe(CH_3OH)('N_HS_4')] (eq 7) or [Fe(THF)('N_HS_4')] (eqs 7 and 8) was identified as a major impurity by IR spectroscopy.

$$2(\mathbf{2}) + N_2H_4 \xrightarrow{CH_3OH\ or\ THF/20°C} [\mu\text{-}N_2H_4\{Fe('N_HS_4')\}_2] \quad (7)$$

$$\mathbf{2} + \mathbf{1} \xrightarrow{THF/20°C} [\mu\text{-}N_2H_4\{Fe('N_HS_4')\}_2] \quad (8)$$

In the course of the investigations described here, a new synthesis of the free ligand 'N_HS_4'–H_2 according to eq 9 was worked out, making it accessible in high yields and pure form. As reported previously,[7] this synthesis proceeds via hydrolysis of [Fe(CO)('N_HS_4')] by aqueous HCl; it is carried out, however, not in THF but in CH_2Cl_2.

$$[Fe(CO)('N_HS_4')] + HCl_{aq,exc} \xrightarrow[3h/40°C]{CH_2Cl_2/-CO} ['N_HS_4'\text{–}H_2]\cdot HCl + FeCl_2 \quad (9)$$

The decisive point of this synthesis is that $FeCl_2$ is insoluble in CH_2Cl_2 such that it can easily be removed in the aqueous phase while ['N_HS_4'–H_2]·HCl remains in the CH_2Cl_2 phase.

X-ray Structure Analyses of [Fe(N_2H_4)('N_HS_4')] (1a), [Fe(CH_3OH)('N_HS_4')] (2), and [Fe(NH_3)('N_HS_4')] (5).

1a, **2**, and **5** were characterized by X-ray structure analyses. Figure 5 shows the molecular structures; selected distances and angles are listed in Table IV.

Analogous to the structurally characterized low-spin complexes [Fe(L)('N_HS_4')] (L = CO,[7] $^1/_2N_2H_2$,[9] NO[8]), the high-spin Fe^{II} centers of **1a**, **2**, and **5** are coordinated pseudooctahedrally by the sulfur and amine donors of the 'N_HS_4'$^{2-}$ ligand and the coligand L. In all cases the four sulfur atoms form planes, and the amine N and L occupy trans positions. In contrast to the low-spin CO and N_2H_2 complexes, the thiolate donors of the 'N_HS_4'$^{2-}$ ligands in **1a**, **2**, and **5** are in cis positions such that a meso configuration results for the [Fe('N_HS_4')] fragments. This meso configuration is also found in the paramagnetic but low-spin 19e$^-$ [Fe(NO)('N_HS_4')].[8]

As Table V shows the Fe–S and Fe–N_H distances of paramagnetic and diamagnetic [Fe(L)('N_HS_4')] complexes vary drastically, in spite of largely similar coordination geometries.

The low-spin 18e$^-$ complexes (L = CO, $^1/_2N_2H_2$) exhibit average Fe–S(thioether), Fe–S(thiolate), and Fe–N(amine) distances of 224, 229, and 205 pm, respectively, that are also found in other Fe^{II} low-spin compounds, e.g., [Fe(9S3)$_2$](PF$_6$)$_2$[16] (224.1–225.9 pm). With regard to these values, the Fe–S(thioether) distances (230.5 and 234.1 pm) and the Fe–N(amine) distance (225.8 pm) of [Fe(NO)('N_HS_4')] are elongated by ca. 8 and 20 pm, respectively. These elongations are even larger in the 18e$^-$ high-spin complexes **1a**, **2**, and **5**, in average reaching 35 pm (Fe–S(thioether)), 10 pm (Fe–S(thiolate)), and 20 pm (Fe–N(amine)), in comparison to the distances in [Fe(CO)('N_HS_4')]. It is noteworthy that the Fe–S(thioether) distances of ca. 259 pm in **1a**, **2**, and **5** are even more than 10 pm longer than in other 18e$^-$ high-spin Fe^{II} complexes, e.g., [Fe(I)$_2$(16S4)] (247.5–248.5 pm).[17] The drastical lengthening of the iron donor atom distances is accompanied by configurational changes of the [Fe('N_HS_4')] fragment. As shown in Figure 6, the thiolate atoms of the 'N_HS_4'$^{2-}$ ligand are in trans positions (Figure 6a) in 18e$^-$ low-spin complexes (L = CO, $^1/_2N_2H_2$), while in all other complexes having longer Fe donor bonds (L = NO, 19e$^-$ low-spin; L = N_2H_4, CH_3OH, NH_3, 18e$^-$ high-spin) the thiolate atoms are in cis positions (Figure 6b).

A plausible reason for this effect may be the tendency of the 'N_HS_4'$^{2-}$ ligand to coordinate the iron centers with the least possible

(13) Gütlich, P. In *Mössbauer Spectroscopy in Chemistry*; Gonser, U., Ed.; Topics in Applied Physics Series; Springer: Berlin, 1975; Vol. 5.
(14) Sellmann, D.; Lanzrath, G.; Huttner, G.; Zsolnai, L.; Krüger, C.; Claus, K. H. *Z. Naturforsch.* **1983**, *38b*, 961.
(15) Goodwin, H. A. *Coord. Chem. Rev.* **1976**, *18*, 293.
(16) Wieghardt, K.; Küppers, H. J.; Weiss, J. *Inorg. Chem.* **1985**, *24*, 3067.
(17) Hills, A.; Hughes, D. L.; Jimenez-Tenorino, M.; Leigh, G. J.; Houlton, A.; Silver, J. *J. Chem. Soc., Chem. Commun.* **1989**, 1774.

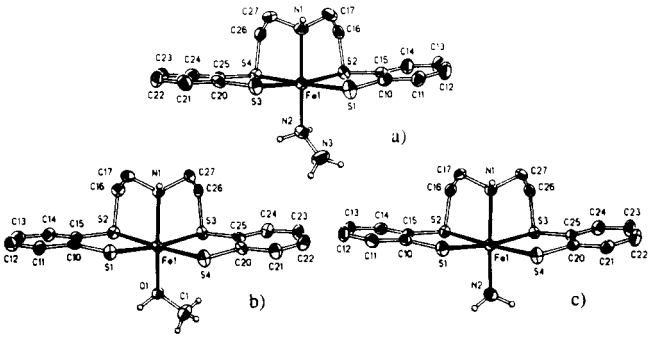

Figure 5. Molecular structures of (a) $[Fe(N_2H_4)('N_HS_4')]$ (**1a**), (b) $[Fe(CH_3OH)('N_HS_4')]$ (**2**), and (c) $[Fe(NH_3)('N_HS_4')]$ (**5**) (H atoms omitted except N_H and coligand H atoms).

Table IV. Selected Distances (pm) and Angles (deg) of $[Fe(N_2H_4)('N_HS_4')]$ (**1a**), $[Fe(CH_3OH)('N_HS_4')]$ (**2**), and $[Fe(NH_3)('N_HS_4')]$ (**5**)[a]

	$[Fe(N_2H_4)('N_HS_4')]$ (**1a**)		
Fe(1)–S(1)	238.1 (3)	Fe(1)–S(2)	260.2 (3)
Fe(1)–S(3)	240.2 (3)	Fe(1)–S(4)	260.2 (3)
Fe(1)–N(1)	225.5 (6)	Fe(1)–N(2)	219.2 (6)
N(2)–N(3)	143.9 (10)	S(1)–C(10)	176.6 (8)
S(2)–C(15)	179.7 (7)	S(2)–C(16)	181.5 (8)
N(1)–C(17)	148.0 (10)	C(16)–C(17)	152.9 (12)
N(2)–Fe(1)–S(1)	97.0 (2)	N(2)–Fe(1)–S(2)	85.6 (2)
S(1)–Fe(1)–S(2)	83.3 (1)	S(1)–Fe(1)–S(3)	98.4 (1)
S(2)–Fe(1)–S(3)	172.3 (1)	S(1)–Fe(1)–S(4)	177.4 (1)
S(2)–Fe(1)–S(4)	94.8 (1)	S(3)–Fe(1)–S(4)	83.3 (1)
N(2)–Fe(1)–N(1)	158.8 (2)	S(1)–Fe(1)–N(1)	96.7 (2)
S(2)–Fe(1)–N(1)	80.0 (2)	Fe(1)–N(2)–N(3)	118.3 (5)
C(17)–N(1)–C(27)	115.3 (6)		
	$[Fe(CH_3OH)('N_HS_4')]$ (**2**)		
Fe(1)–S(1)	238.7 (2)	Fe(1)–S(2)	257.8 (2)
Fe(1)–S(3)	258.2 (3)	Fe(1)–S(4)	238.3 (2)
Fe(1)–N(1)	220.3 (7)	Fe(1)–O(1)	211.0 (6)
S(1)–C(10)	176.2 (8)	S(2)–C(15)	179.7 (8)
S(2)–C(16)	182.2 (9)	N(1)–C(17)	149.0 (11)
C(16)–C(17)	151.6 (13)	C(1)–O(1)	142.2 (11)
S(1)–Fe(1)–S(2)	84.2 (1)	S(1)–Fe(1)–S(3)	172.3 (1)
S(2)–Fe(1)–S(3)	94.8 (1)	S(1)–Fe(1)–S(4)	97.2 (1)
S(2)–Fe(1)–S(4)	177.3 (1)	S(3)–Fe(1)–S(4)	83.5 (1)
S(1)–Fe(1)–N(1)	91.5 (2)	S(2)–Fe(1)–N(1)	82.0 (2)
S(1)–Fe(1)–O(1)	100.9 (2)	S(2)–Fe(1)–O(1)	87.9 (2)
C(17)–N(1)–C(27)	115.0 (6)	N(1)–C(17)–C(16)	112.7 (7)
Fe(1)–O(1)–C(1)	127.6 (5)		
	$[Fe(NH_3)('N_HS_4')]$ (**5**)		
Fe(1)–S(1)	239.7 (2)	Fe(1)–S(2)	258.8 (2)
Fe(1)–S(3)	258.6 (2)	Fe(1)–S(4)	239.4 (2)
Fe(1)–N(1)	224.4 (3)	Fe(1)–N(2)	218.9 (3)
S(1)–C(10)	176.3 (4)	S(2)–C(15)	177.9 (4)
S(2)–C(16)	181.3 (4)	N(1)–C(17)	148.9 (5)
C(16)–C(17)	153.0 (6)		
S(1)–Fe(1)–S(2)	83.8 (1)	S(1)–Fe(1)–S(3)	171.2 (1)
S(2)–Fe(1)–S(3)	95.2 (1)	S(1)–Fe(1)–S(4)	97.0 (1)
S(2)–Fe(1)–S(4)	176.5 (1)	S(3)–Fe(1)–S(4)	83.6 (1)
S(1)–Fe(1)–N(1)	91.1 (1)	S(2)–Fe(1)–N(1)	81.3 (1)
S(1)–Fe(1)–N(2)	101.6 (1)	S(2)–Fe(1)–N(2)	89.6 (1)
N(1)–Fe(1)–N(2)	163.5 (1)	N(1)–C(17)–C(16)	112.0 (3)

[a] Estimated standard deviations are given in parentheses.

steric strain. This assumption is corroborated by the observation that, in spite of drastic changes of the iron donor distances of up to 35 pm, the distances and angles within the $(C_2H_4)_2NH$ bridge remain nearly unchanged. Thus, the C–N distances in the bridges of all complexes exhibit an average value of 148.5 pm with a maximum deviation of 1.7 pm, and the C–N–C angles of the bridge reveal an average value of 114.8° with a maximum deviation of 1.3°.

Discussion

Comparison of the $[Fe(L)('N_HS_4')]$ complexes characterized so far reveals the following points: (1) All complexes, except the 19e⁻ complex $[Fe(NO)('N_HS_4')]$, have 18e⁻ configurations. (2) The σ donor coligands THF, CH_3OH, or N_2H_4 yield paramagnetic high-spin complexes having four unpaired electrons. The σ–π coligands CO, $P(OPh)_3$, or N_2H_2, however, lead to the formation of diamagnetic low-spin complexes. (3) All high-spin complexes are highly reactive; all low-spin complexes are comparatively inert with respect to substitution or oxidation by air. (4) As shown in Table V, the Fe–S– and Fe–N_H distances within the $[Fe('N_HS_4')]$ fragments drastically increase when going from the low-spin 18e⁻ complexes, via the 19e⁻ low-spin complex $[Fe(NO)('N_HS_4')]$ that takes an intermediate position, to the 18e⁻ high-spin complexes.

Magnetic and electronic, and structural and reactive properties of $[Fe(L)('N_HS_4')]$ compounds are evidently coupled strongly. The coligands L determine the spin state of the iron centers, and the $[Fe('N_HS_4')]$ fragment electronically appears to be in a border situation, where small changes like the substitution of only one ligand lead to spin crossovers. In this respect $[Fe(L)('N_HS_4')]$ complexes compare with those Fe^{II} compounds whose magnetism also depends on coligands and sometimes only on temperature.[18]

The relation among magnetism, structure, and reactivity of $[Fe(L)('N_HS_4')]$ complexes can be explained in terms of molecular orbital theory. In order to simplify matters, the $[Fe(L)('N_HS_4')]$ complexes are assumed to posses ideal octahedral symmetry and to exclusively exhibit σ bonds in the $[Fe('N_HS_4')]$ fragment. If L, too, is a σ donor, the familiar MO scheme of octahedral complexes with σ ligands results.[19] The t_{2g} orbitals are of pure metal character, and the e_g^* orbitals are antibonding with respect to metal ligand bonds (Figure 7a). Substitution of one σ ligand by a σ–π ligand such as CO results in the MO scheme in Figure 7b. Interaction of π and π^* orbitals of the σ–π ligand with the t_{2g} orbitals lifts the degeneracy of the t_{2g} orbitals, two of them being lowered in energy. Simultaneously, the energy gap between the remaining metal orbital a_M and the lowest antibonding metal ligand orbitals e^*_σ becomes larger.[19]

As a consequence, the sequence and population of frontier orbitals, according to the scheme in Figure 8, are to be expected. This scheme plausibly explains why complexes with σ coligands have high-spin Fe^{II} centers and four unpaired electrons. Two of these electrons have to occupy e_g^* orbitals, being antibonding with respect to metal ligand bonds (Figure 8a). Quite accordingly, 18e⁻ complexes with σ–π ligands are diamagnetic and fairly inert because they have no electrons in antibonding orbitals (Figure 8b). Finally, $[Fe(NO)('N_HS_4')]$ also can be accommodated in the scheme. The σ–π ligand NO causes the expected low-spin configuration, but because neutral NO acts as a 3e⁻ donor, a 19e⁻ configuration results and the unpaired 19th electron has to occupy one of the antibonding e_σ^* orbitals (Figure 8c).

Thus, the increasing occupation of antibonding orbitals explains the increase in bond lengths when going from the 18e⁻ low-spin, via the 19e⁻ low-spin complex $[Fe(NO)('N_HS_4')]$, to the 18e⁻ high-spin complexes.

Simultaneously the reason for the drastically different reactivities of the high- and low-spin complexes becomes clear. The breakage of iron coligand bonds, being necessary in substitution reactions, is expected to require considerably lower activation energies in the high-spin compounds having long metal donor bonds than in low-spin compounds having short and strong metal donor bonds.

Summary

Iron complexes with a coordination sphere dominated by sulfur can serve as model compounds for the active centers of nitrogenases

(18) a) Gütlich, P. Spin-Crossover in Iron(II) Complexes. *Struct. Bonding (Berlin)* **1981**, *44*, 83. b) Bacci, M. *Coord. Chem. Rev.* **1988**, *86*, 245.
(19) Albright, T. A.; Burdett, J. K.; Whangbo, M. H. *Orbital Interactions in Chemistry*; Wiley: New York, 1985.

Table V. Bond Distances (pm) and Magnetic Moments μ_{eff} (μ_B) of Low-Spin and High-Spin [Fe(L)('N_HS_4')] Complexes

	L = CO[7]	L = $^1/_2(N_2H_2)$[a]	L = NO[8]	L = CH_3OH	L = N_2H_4	L = NH_3
d(Fe–S(thioether))	222.5 (3)	223.4 (1)	234.1 (3)	257.8 (2)	260.2 (3)	258.8 (2)
	225.1 (3)	225.1 (1)	230.5 (2)	258.2 (3)	260.2 (3)	258.6 (2)
d(Fe–S(thiolate))	229.8 (3)	231.8 (2)	229.7 (3)	238.7 (2)	238.1 (3)	239.7 (2)
	230.5 (3)	228.8 (2)	227.2 (3)	238.3 (2)	240.2 (3)	239.4 (2)
$d(Fe–S)_{av}$	227.0	227.3	230.4	248.3	249.7	249.2
d(Fe–N(amine))	207.2 (8)	203.7 (4)	225.8 (7)	220.3 (7)	225.5 (6)	224.4 (3)
μ_{eff}	0	0	2.13	4.88	4.98	cf. text

[a] The N_2H_2 complex is dinuclear [μ-N_2H_2{Fe('N_HS_4')}$_2$].[9]

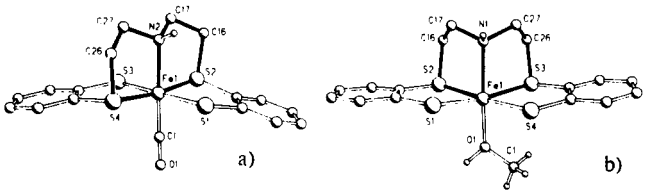

Figure 6. Trans and cis coordination of 'N_HS_4'$^{2-}$ thiolate donors in (a) 18e$^-$ low-spin [Fe(CO)('N_HS_4')] and (b) 18e$^-$ high-spin [Fe(CH_3OH)('N_HS_4')].

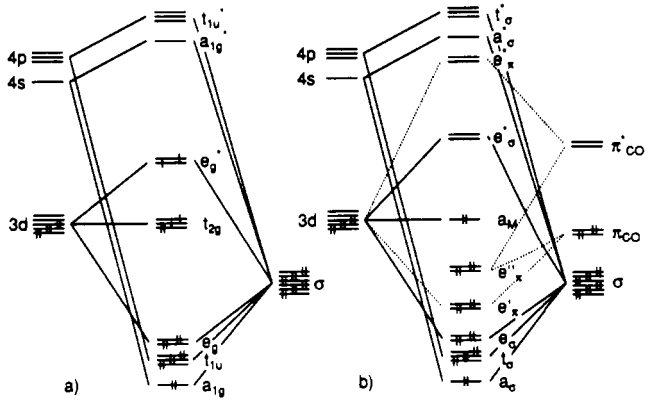

Figure 7. Simplified MO diagrams for [Fe(L)('N_HS_4')] complexes with (a) σ coligands L and (b) σ–π coligands L.

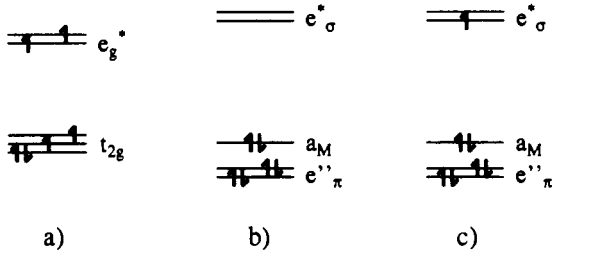

Figure 8. Sequence and population of frontier orbitals in [Fe(L)('N_HS_4')] complexes with (a) 18e$^-$ high-spin, (b) 18e$^-$ low-spin, and (c) 19e$^-$ low-spin configurations.

because of their chemical composition. The [Fe(L)('N_HS_4')] complexes described above demonstrate that the [Fe('N_HS_4')] fragment is able to bind either hard σ ligands like N_2H_4 or soft σ–π ligands like N_2H_2. In this respect, the [Fe('N_HS_4')] fragment is electronically as well as chemically highly flexible. This distinguishes the [Fe('N_HS_4')] fragment from numerous other complex fragments, in which the metal centers are largely determined by the ligand spheres to be either hard *or* soft.

The flexibility of the [Fe('N_HS_4')] fragment can be traced back to the 'N_HS_4'$^{2-}$ ligand. It exhibits three types of donors: the hard N_H, the intermediate S thioether, and the soft S thiolate ligands. While N_H can only act as a σ donor, for thioether S atoms additionally π acceptor and for thiolate S atoms π donor abilities have to be considered. Combination of these different types of donors in one pentadentate chelate ligand and the [Fe('N_HS_4')] coordination sphere, respectively, allows drastic changes of the metal ligand bonds and simultaneously prevents total and irreversible dissociation of the corresponding complexes.

Scheme I

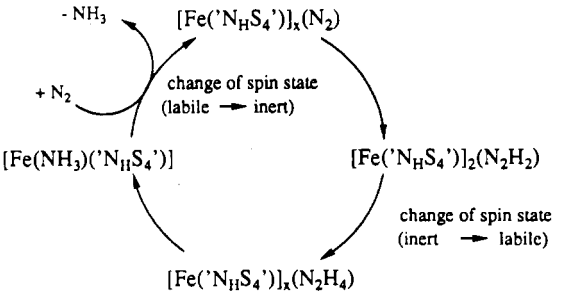

In this respect the 'N_HS_4'$^{2-}$ ligand and the [Fe('N_HS_4')] fragment exhibit properties which can also be expected from peptide chains in natural systems when they coordinate metals. These act as multidentate ligands in metalloenzymes and allow not only specific reactivities, but also unusual coordination geometries, e.g., in plastocyanins.[20]

The [Fe(L)('N_HS_4')] complexes described above are of special interest as model compounds for the active centers of nitrogenases. The discovery of nitrogenases containing exclusively iron makes iron complexes with sulfur-dominated coordination spheres suitable model compounds, especially if they posses sites for the coordination of N_2 or its reduction products N_2H_2, N_2H_4, and NH_3. The coordination of N_2 could not yet be achieved, but the series with L = N_2H_2, N_2H_4, and NH_3 was obtained.

Scheme I outlines how in a catalytic cycle two spin-state changes, connected with a change from substitution inert to substitution labile complexes and vice versa, not only may possibly assist the reduction steps leading from N_2 via N_2H_2 and N_2H_4 to NH_3, but also will certainly favor the final step when NH_3 is substituted by N_2. It is furthermore noteworthy that this cycle comprises Fe^{II} complexes only such that no extraordinary oxidation states, e.g., Fe^I or Fe^0 have to be assumed.

Acknowledgment. We gratefully acknowledge the support of these investigations by the Deutsche Forschungsgemeinschaft, the Bundesministerium für Forschung und Technologie, and the Fonds der Chemischen Industrie.

Supplementary Material Available: Tables of crystallographic data and data collection parameters, all bond lengths and bond angles, anisotropic thermal parameters, and fractional coordinates of hydrogen atoms (15 pages); listings of calculated and observed structure factors (35 pages). Ordering information is given on any current masthead page. Further details of the X-ray crystal structure analyses have been deposited and can be obtained from the Fachinformationszentrum Karlsruhe, D-7514 Eggenstein-Leopoldshafen 2, Federal Republic of Germany, by citing the deposition nos. CSD 320386 ([Fe(N_2H_4)('N_HS_4')] (**1a**)), CSD 320385 ([Fe(CH_3OH)('N_HS_4')] (**2**)), and CSD 320084 ([Fe(NH_3)('N_HS_4')] (**5**)), the authors, and the reference.

(20) Cotton, F. A.; Wilkinson, G. *Advanced Inorganic Chemistry*, 5th ed.; Wiley: New York, 1988.